Vergnes, Laurent and Davies, Graeme R. and Lin, Jason Y. and Yeh, Michael W. and Livhits, Masha J. and Harari, Avital and Symonds, Michael E. and Sacks, Harold S. and Reue, Karen (2016) Adipocyte browning and higher mitochondrial function in peri-adrenal but not subcutaneous fat in pheochromocytoma. Journal of Clinical Endocrinology and Metabolism . jc.2016-2670. ISSN 1945-7197

Adipocyte browning and higher mitochondrial function in peri-adrenal but not subcutaneous fat in pheochromocytoma.

Laurent Vergnes[1*], Graeme R. Davies[2*], Jason Y. Lin[1], Michael W. Yeh[3], Masha J. Livhits[3], Avital Harari[3], Michael E. Symonds[2], Harold S. Sacks[4], Karen Reue[1,5]

[1]Department of Human Genetics, David Geffen School of Medicine, University of California, Los Angeles, Los Angeles, CA;

[2]Academic Division of Child Health, Obstetrics and Gynaecology, School of Medicine, Queen's Medical Centre, The University of Nottingham, Nottingham, NG7 2UH, UK;

[3]Section of Endocrine Surgery, UCLA David Geffen School of Medicine, Los Angeles, CA;

[4]Endocrinology and Diabetes Division, VA Greater Los Angeles Healthcare System, Department of Medicine, University of California, Los Angeles, David Geffen School of Medicine, Los Angeles CA;

[5]Molecular Biology Institute, University of California, Los Angeles, Los Angeles, CA.

[*] Contributed equally to this study

Abbreviated title: Mitochondrial activity in pheochromocytoma

Key term: pheochromocytoma, adipocyte browning, mitochondrial respiration

Word count: 3620

Number of figures and tables: 6

Corresponding author and person to whom reprint requests should be addressed:

Laurent Vergnes

Department of Human Genetics, David Geffen School of Medicine

University of California, Los Angeles

695 Charles E. Young Dr south, Los Angeles, CA 90095.

Phone: 1-310-267-2741.

Fax: 1-310-794-5446.

Email: lvergnes@ucla.edu

Funding: This work was supported by the Fondation Leducq 12CVD04 (L.V., K.R.), NIH P01 HL28481 (K.R.), the National Center for Research Resources Grant S10RR026744 (K.R.).

Disclosure statement: The authors have nothing to disclose.

Abstract

Context: Patients with pheochromocytoma (pheo) show presence of multilocular adipocytes that express uncoupling protein (UCP) 1 within periadrenal (pADR) and omental (OME) fat depots. It has been hypothesized that this is due to adrenergic stimulation by catecholamines produced by the pheo tumors.

Objective: To characterize the prevalence and respiratory activity of brown-like adipocytes within pADR, OME and subcutaneous (SC) fat depots in human adult pheo patients.

Design: This was an observational cohort study.

Setting: University hospital.

Patients: We studied 46 patients who underwent surgery for benign adrenal tumors (21pheos and 25 controls with adrenocortical adenomas).

Main outcome measure: We characterized adipocyte browning in pADR, SC, and OME fat depots for histological and immunohistological features, mitochondrial respiration rate, and gene expression. We also determined circulating levels of catecholamines and other browning-related hormones.

Results: 11 of 21 pheo pADR adipose samples, but only 1 of 25 pADR samples from control patients, exhibited multilocular adipocytes. The pADR browning phenotype was associated with higher plasma catecholamines and raised UCP1. Mitochondria from multilocular pADR fat of pheo patients exhibited increased rates of coupled and uncoupled respiration. Global gene expression analysis in pADR fat revealed enrichment in β-oxidation genes in pheo patients with multilocular adipocytes. No SC or OME fat depots exhibited aspects of browning.

Conclusion: Browning of the pADR depot occurred in half of pheo patients and was associated with increased catecholamines and mitochondrial activity. No browning was detected in other fat depots, suggesting that other factors are required to promote browning in these depots.

Introduction

Evidence for the presence of functional brown adipose tissue (BAT) in humans (1–4) rekindled research into the proposal made more than 30 years earlier that the high fat-oxidizing, energy-expending capacity of BAT might be exploited to treat obesity (5). The hallmark property of BAT that promotes energy expenditure is the expression of uncoupling protein (UCP)1, a mitochondrial transporter that creates proton leaks across the inner mitochondrial membrane, leading to the dissipation of energy as heat (6). Positron emission tomography-computed tomography (PET/CT) imaging revealed that fat depots in the supraclavicular region exhibit high [^{18}F]-fluorodeoxyglucose uptake, suggesting high metabolic activity (2–4) that was increased upon cold exposure (4). Potential strategies to increase energy expenditure include activation of established BAT depots or induction of brown adipocyte progenitors within white adipose tissue (WAT) depots using pharmacological or environmental stimuli (7–9). Thus far, there is limited evidence regarding whether humans have the potential for appreciable induction of metabolically active brown adipocytes within WAT.

Studies in mice have revealed that "classical" brown adipocytes from the interscapular adipose depot are derived from a cell lineage that is distinct from white adipocytes. Brown adipocytes derive from a Myf5^{+} lineage, whereas brown-like adipocytes that are induced within WAT (referred to as "beige" or "brite" cells) originate preferentially from Myf5^{-} progenitor cells (10). Brown and beige adipocytes have distinct molecular and developmental characteristics, but the mitochondrial and regulatory differences are not fully understood. In humans, fat depots that exhibit a brown/beige gene expression signature include the supraclavicular, paravertebral, perirenal and epicardial fat depots. These fat depots appear to be a mixture of brown and/or beige adipocytes embedded within WAT (7,11–15). The identification of specific markers for brown *vs.* beige adipocytes has been difficult due to a lack of pure brown or beige fat samples, as well as possible differences between humans and mice.

Pheochromocytoma (pheo) is a catecholamine-secreting neoplasm arising primarily from the adrenal medulla or within paragangliomas (16). Multilocular adipocytes with UCP1 expression have been detected in pheo patients in perirenal fat (17–20) and OME fat (21,22), but not in subcutaneous (SC) adipose tissue (19,22), These studies have been constrained by very small samples sizes. In addition, the browning in perirenal and OME fat does not seem to occur in all pheo patients, and may be as low as 50-60% (18,21). At present, it is unknown whether the brown-like adipocytes that occur in WAT of some pheo patients exhibit metabolic changes that are characteristic of brown adipocytes, such as increased mitochondrial function and uncoupled respiration.

In the present study, we have characterized multiple WAT depots from pheo subjects and control subjects with non-catecholamine secreting adrenal tumors i) to determine the prevalence of browning in different anatomical WAT depots; and ii) to determine whether pheo-associated WAT browning is associated with increased mitochondrial respiration activity.

Materials and Methods

Human subjects

The study protocol was reviewed and approved by the University of California Los Angeles Medical Institutional Review Board. Each patient provided written consent after the study goals, side effects and tissue sampling procedure were explained in detail. Patients in the experimental group had sporadic unilateral benign adrenal pheos (i.e., no family history of a pheo). Pheo patients were routinely prepared pre-operatively with a 2-4 week course of the long-acting α-adrenergic receptor blocking drug phenoxybenzamine supplemented, when needed, with β-blockers. Patients in the control group had aldosterone– or cortisol-secreting, or non-functioning neoplasms. Exclusion criteria were (i) Paragangliomas, (ii) malignant tumor, (iii) type 2 diabetes treated with a thiazolidinedione, or (iv) untreated hyper- or hypothyroidism.

Fat biopsies were removed after tumor resection under stable intraoperative hemodynamic conditions. Depending on the surgical approach taken to perform adrenalectomy, ~1 g was resected from superficial SC fat in the anterior upper abdomen or in the posterior abdominal wall below the 12th rib. 1-3 g was taken from retroperitoneal fat adjacent to the adrenal tumor. When the operative approach was intra-peritoneal, 1-3 g OME fat was also collected. Fat samples were placed on ice and processed within 30 min of collection. After cleaning, fat samples were cut into pieces and used fresh for bioenergetics experiments, fixed in formalin for histology, or snap frozen in liquid nitrogen and stored at –80ºC.

Blood collection and analyses

Fasting blood was collected between 7 am and 10 am in EDTA tubes from patients just before entering the operating room. Plasma aliquots were sent to Quest Diagnostics to measure fractionated catecholamines by HPLC or stored at –80ºC. Plasma glucose concentrations were measured using a colorimetric glucose assay kit (GAGO-20, Sigma Aldrich). Atrial natriuretic peptide (ANP) (EIA-ANP, RayBiotech, Inc.), B-type natriuretic peptide (BNP) (ELH-BNP, RayBiotech, Inc.), and cortisol (ADI-900-071, Enzo) were measured according to the manufacturer's instructions. For cortisol determination, steroid displacement reagent was used to displace steroid binding to proteins.

Histology

Haemotoxylin and eosin staining was performed on 7 µm sections from each fat depot. Several sections from different regions of each biopsy were evaluated. The presence of unilocular and multilocular adipocytes in each section was assessed visually by bright-field microscopy by 2-3 independent observers.

Immunohistochemistry

The presence of UCP1 protein in tissue samples was assessed by immunohistochemistry with a UCP1 antibody (#662045, Calbiochem) at 1:500 dilution. Staining specificity was confirmed on slides where primary antibody was omitted. Sections were counterstained with hematoxylin.

Gene expression analysis

RNA was extracted from frozen tissue samples using TRIzol (Life Technologies). For real-time quantitative PCR analysis (RT-qPCR), 1 µg of RNA was reverse transcribed using iScript (Bio-Rad). A standard curve was constructed from pooled cDNA samples to take account the efficiency of primers and to obtain the Standard Quality (SQ) values. Target gene SQ values were normalized to B2M and 36B4, which did not differ significantly between the groups. Primer sequences are listed in Supplemental Table 1.

For global gene expression, RNA from pADR fat depots was arrayed on an Illumina HT-12 v4.0 bead chip at the UCLA Neuroscience Genomics Core. Analysis was performed with GenomeStudio V2011.1 using quantile normalization, background subtraction, and a present call $P < 0.05$. Differentially regulated genes were defined as having > 2-fold difference compared to control. Lists of genes that were significantly up- or down-regulated were subjected to functional enrichment using DAVID annotation tools and the "single protein of protein information resource" (SP_PIR) category (23). Venn analysis and heat map representations were obtained with GenePattern (genepattern.broadinstitute.org).

Protein analysis by Western blotting

Western blots were performed essentially as published previously (14) with minor changes. Briefly, 8 µg mitochondrial protein extracts were separated by SDS-PAGE and transferred to a nitrocellulose membrane. After blocking in 5% milk and 0.2% Tween 20 in TBS, anti-UCP1 antibody (1:1000 dilution, #662045, Calbiochem) was incubated overnight at 4ºC in

3% milk and 0.2% Tween 20 in TBS. An anti-cytochrome c antibody (136F3, Cell Signalling Technology®) was used in 5% bovine serum albumin and also incubated overnight. A goat anti-rabbit secondary antibody (sc-2030, Santa Cruz Biotechnology, Inc.) was used at 1:20,000 dilution for 1h at room temperature. Immunoreactive bands were developed with ECL Prime (RPN2232, Amersham) and visualized with a Bio-Rad Gel-Doc imager.

Mitochondrial Bioenergetics

Mitochondria were isolated from fresh tissues and immediately used in an XF24 Analyzer (Seahorse Bioscience) as previously described (24). Briefly, mitochondrial protein yield was determined by Bradford assay and 50 µg pADR or 100 µg SC or OME mitochondria were seeded per well by centrifugation. For the coupling assay, basal oxygen consumption rate (OCR) was measured in the presence of 10 mM succinate and 2 µM rotenone, and after sequential addition of 4 mM ADP (Complex V substrate), 2.5 µg/ml oligomycin (Complex V inhibitor), 4 µM FCCP (mitochondrial uncoupler) and 4 µM antimycin A (Complex III inhibitor). For electron flow assays, basal OCR was measured in presence of 10 mM pyruvate (Complex I substrate), 2 mM malate and 4 µM FCCP, and after sequential addition of 2 µM rotenone (Complex I inhibitor), 10 mM succinate (Complex II substrate), 4 µM antimycin A (Complex III inhibitor) and 1mM TMPD containing 10 mM ascorbate (Complex IV substrate). OCR was normalized per µg mitochondrial protein.

Statistics

Statistical analyses were performed with GraphPad Prism. Normal distribution of samples was tested to select parametric or nonparametric tests as indicated in the figure legends. Two-tailed Student's *t* test or one-way ANOVA for multiple comparisons was used to determine *P* values. Pearson's coefficient correlation (r) and *P* values were calculated for the linear

correlations. All results are expressed as mean ± SEM or mean ± SD for subject characteristics. Statistical significance was defined as $P < 0.05$.

Results

Forty-six patients with benign adrenal tumors were enrolled in the study; clinical characteristics are presented in Table 1. Of these, 21 tumors were confirmed to be pheos on histopathology and 25 were adrenal cortical adenomas, which served as controls. The controls included 12 aldosterone-secreting adenomas, 2 cortisol-secreting adenomas, and 11 non-functioning tumors. The mean age, plasma glucose and free fatty acid levels were not different between the pheo and control groups. Body mass index (BMI) was lower in the pheo group compared to controls ($P = 0.048$).

Histology was performed for pADR and SC fat samples from all patients (21 pheos, 25 controls). OME fat was collected only from individuals having intra-peritoneal surgery, leading to availability of OME samples from only 5 control and 4 pheo patients. All sections examined from OME and SC depots contained adipocytes with unilocular morphology. In pADR samples, multilocular adipocytes characteristic of brown/beige adipose tissue were present in 52.4% (11/21) of pheo samples, but in only 4% (1/25) of the controls ($P < 0.001$, Fisher's exact test). Typically, the multilocular adipocytes in pADR fat occurred in pockets that were dispersed throughout the white adipocytes (Figure 1 and Supplemental Fig. 1). Based on histology, we classified pheo subjects for subsequent analysis as either pheo^{Uni} (having exclusively unilocular adipocytes) or pheo^{Multi} (having some multilocular adipocytes).

The control, pheo^{Uni}, and pheo^{Multi} groups did not differ in age, BMI, or plasma glucose and free fatty acid levels (Table 1). Atrial (ANP) and B-type (BNP) natriuretic peptides, as well as cortisol levels, have been associated with browning in WAT depots (25–27). Plasma levels of these hormones did not differ among the three groups of patients (Table 1), suggesting no

influence on browning in the pheo^{Multi} group. In addition, use of β-blockers was equally divided between pheo^{Uni} and pheo^{Multi} (5/10 and 5/11 patients, respectively) thus ruling out an inhibitory effect of the β-adrenergic blockers on adipocyte browning. We hypothesized that differences in catecholamine levels released by the adrenal tumors may influence the development of multilocular adipocytes. The pheo^{Multi} group had higher total and individual plasma catecholamines (norepinephrine, epinephrine, normetanephrine and metanephrine) than the control group (Figure 2). Notably, the pheo^{Multi} group had higher total catecholamine and norepinephrine levels than the pheo^{Uni} group. The pheo^{Uni} group also showed significantly higher normetanephrine and metanephrine levels than controls, but the levels were not as high as in the pheo^{Multi} group. Thus, the pheo^{Multi} patients had higher levels than control subjects for all catecholamines measured, and were distinguished from the pheo^{Uni} subjects by higher total catecholamine levels.

We examined UCP1 mRNA and protein levels in adipose tissue from pADR, SC and OME depots. UCP1 mRNA abundance was significantly higher in pADR fat from the pheo^{Multi} group compared to the control (9-fold) and the pheo^{Uni} (24-fold) groups (Figure 3A). By contrast, UCP1 mRNA levels in SC or OME depots were low and not different between the three patient groups. Immunohistochemistry localized UCP1 protein exclusively to multilocular adipocytes within the pADR fat samples (Figure 3B). No UCP1 staining was observed in pADR fat from control or pheo^{Uni} groups, or in OME or SC fat depots from any group. By Western blot analysis, we detected UCP1 protein in pADR fat from individuals in the pheo^{Multi} group, but not in the pheo^{Uni} or control groups (Figure 3C). No UCP1 protein was detected in SC or OME fat from any group (data not shown).

The presence of multilocular adipocytes expressing *UCP1* in pADR fat from pheo patients has been reported previously (17–20), but it has not been determined whether these adipocytes exhibit enhanced mitochondrial function. To evaluate, we isolated mitochondria from

the pADR, SC, and OME fat depots of control, pheo^{Uni}, and pheo^{Multi} groups and measured total respiration and activity of specific mitochondrial respiratory chain complexes. First, using a coupling assay, basal oxygen consumption rate (OCR) was 7-fold higher in mitochondria from pADR fat of pheo^{Multi} subjects than from the other groups (Figure 4A), whereas in SC and OME fat depots it was similar in all groups. Complex V and maximal respiration rates were also raised in the pheo^{Multi} group (Figure 4B) as was coupled and uncoupled respiration rates. Finally, we assessed the activity of the respiratory chain complexes I-IV by performing an electron flow assay. We detected increased OCR for all four complexes in pheo^{Multi} mitochondria compared to both control and pheo^{Uni} groups, while pheo^{Uni} and control groups did not differ from one another (Figure 4C). Overall, these results demonstrate that mitochondria from the pADR fat of pheo^{Multi} patients have higher electron transport chain (ETC) activity and capacity.

To evaluate the relationship between *UCP1* and mitochondrial uncoupling, we assessed the Pearson's correlation between the two traits in all pheo patients. There was a significant positive correlation between UCP1 mRNA levels and uncoupled respiration rate ($r = 0.536$; $P < 0.05$). Correlations between total catecholamines and mitochondrial ETC respiratory chain complex I ($r = 0.743$; $P < 0.01$), complex II ($r = 0.802$; $P < 0.01$), complex III ($r = 0.806$; $P < 0.01$), and IV ($r = 0.762$; $P < 0.01$) were each significant, suggesting an association between plasma catecholamines and mitochondrial activity.

To provide an unbiased assessment of transcriptional changes that lead to enhanced mitochondrial activation in pADR fat of pheo^{Multi} samples, we performed gene expression profiling. We analyzed pADR adipose tissue mRNA from control, pheo^{Uni}, and pheo^{Multi} samples ($n = 4$ patients from each group) by microarray hybridization. Compared to controls, pheo^{Multi} samples showed 2-fold up-regulation of 470 genes and down-regulation of 274 genes ($P < 0.05$); pheo^{Uni} samples showed up-regulation of 590 and down-regulation of 272 genes (Figure 5A). Most relevant to the observed differences in mitochondrial activation between pheo^{Multi} and

pheo^{Uni} groups, 260 genes were uniquely up-regulated, and 188 genes uniquely down-regulated, in pheo^{Multi} fat (Figure 5A, shaded region).

We performed functional annotation of the genes that were specifically altered in the pheo^{Multi} group (shaded regions in Figure 5A) using the DAVID functional annotation tool (23). The genes that were specifically up-regulated in pheo^{Multi} pADR fat were enriched in mitochondrion- and oxidation reduction-related categories (Figure 5A). The genes that were uniquely down-regulated in pheo^{Multi} pADR fat were enriched in categories that include signaling, secreted proteins, and cytokines (Figure 5B). The heat map in Figure 5B displays the expression pattern of the 82 up-regulated genes present in the top enrichment category, mitochondrion ($P <$ 1.82E-48). Genes in this category were associated with the TCA cycle (*ACO2, L2HGDH, DLAT, PDHX*), β-oxidation (*ACAA2, ACADM, CPT1B, HADHA, HADHB*) and respiration (*BRP44, CABC1, ETFDH, SFXN4, UCP1*). Notably, several genes were components of the electron transport chain complex I (*NDUFA8*, *NDUFA9*, *NDUFS3*, *NDUFV3*), complex II (*SDHA* and *SDHB*), complex III (*CYC1*, *COQ3*, *COQ6*, *COQ9*), coenzyme Q complex (*UQCRB*, *UQCRC1*, *UQRC2*, *UQCRFS1*), and complex IV (*COX5A*, *COX6A1*, *COX7B*). We validated expression levels of several genes and proteins by RT-qPCR or western blot. ETC-related gene expression levels were significantly higher in the pheo^{Multi} compared to the control group (Figure 5C). These gene expression differences, together with increased mitochondrial activity, suggest that mitochondria in pheo^{Multi} pADR adipose tissue are altered to promote higher β-oxidation and respiration.

The expression of specific gene markers has been proposed to distinguish brown adipocytes from beige adipocytes (7,15,28–31). We assessed representative brown and beige gene expression markers in pADR fat in our control, pheo^{Uni}, and pheo^{Multi} samples using the microarray data or by RT-qPCR (Supplemental Table 2). Of 17 genes assessed in pADR, only *PAT2* exhibited higher expression in pheo^{Multi} compared to the other groups. These data suggest

that the multilocular adipocytes in pADR fat do not exhibit a typical classical brown or beige adipose tissue gene expression signature.

Discussion

In the present study, we analyzed the effects of increased catecholamine levels present in pheo patients on browning of adipose tissue depots located adjacent to and distant from the pheo tumors. In our sample, which represents the largest series of pheo patients analyzed for effects on browning reported to date, we identified multilocular adipocytes that express *UCP1* in approximately half of the pheo subjects. Adipocytes with brown character were detected in pADR fat, but not in SC or OME adipose tissue depots, which are anatomically distant from the pheo tumor. The subset of pheo patients that exhibited multilocular adipocytes containing UCP1 had higher plasma catecholamine levels than pheo patients that did not exhibit multilocular pADR fat and control subjects with non-catecholamine-secreting adrenal tumors. We demonstrate, for the first time, that the browning phenotype occurring in pADR fat of pheo subjects is associated with elevated mitochondrial respiration, characterized by increased activity of all ETC complexes, as well as increased uncoupled respiration. The increased mitochondrial respiration was associated with elevated expression of a panel of genes involved in mitochondrial energy metabolism.

Pheochromocytoma is a catecholamine-secreting tumor, but there is variation among patients in the levels of circulating catecholamines and in the time between tumor formation and removal, which may be several years (16). Our detection of browning in pADR fat of 11/25 of pheo patients is consistent with a previous study where 62% of pheo cases (5/8) had multilocular adipocytes (18). Notably, we found that the induction of browning did not extend to SC or OME fat depots despite the fact that the catecholamines secreted by the adrenal tumors enter the systemic circulation. In mice, the SC fat depot is susceptible to browning, but may have less capacity to undergo remodeling in humans (9). For example, in a previous study of eight pheo

patients, multilocular adipocytes were visible in the pADR fat but not the SC depot (19). Similarly, no browning was detected in abdominal fat after 8h cold exposure in overweight human adults under conditions that activated BAT glucose metabolism and increased energy expenditure (32). Healthy human volunteers exposed to 10 days of cold also did not show SC browning despite elevated plasma catecholamines (33). In contrast, using major burn trauma as a model for adrenergic stress, multilocular adipocytes expressing *UCP1* in SC fat were observed after only 3 weeks (34,35). Increased *UCP1* expression (3-fold) was also observed in SC fat during winter (36). There are some reports of browning in OME fat in a portion of pheo patients (21,22) but plasma catecholamines were not reported, making it difficult to compare to the current study. Variations in browning in pheo patients could be due to catecholamines, genetic, and/or environmental factors that differ among individuals (e.g., seasonal temperature at the time samples were obtained).

The induction of browning in pheo subjects appears to be adipose depot-dependent, with pADR, and to a lesser extent OME fat depots, more prone to adipose tissue remodeling than SC fat. These findings could have important repercussions on the use of thermogenic agonists to modulate obesity since the majority of human fat is stored in SC depots (37). Differences in vascularization, innervation, or intrinsic properties of adipocyte precursor cells could contribute to differences in the capacity for browning among adipose depots together with mitochondrial capacity to increase respiratory activity, a prominent feature of pADR fat of pheo patients that exhibited browning. We also cannot rule out the possibility that elevated local catecholamine levels adjacent to the tumor play a role in the browning of pADR fat in pheo patients.

Molecular markers for classical brown adipocytes *vs*. beige adipocytes have been identified in mice, and have also been used to characterize human brown/beige cells (7,11–13,15,30,38). By measuring several of these mRNA markers we did not observe a clear classical brown or beige signature in pADR of pheo^{Multi} patients. It should be noted that the use of these gene expression markers to distinguish brown and beige adipocytes remains controversial and

inconclusive. We cannot rule out that the heterogeneity of the pADR tissue, containing regions of typical white adipocytes neighboring the pockets of multilocular adipocytes, may prevent definitive gene expression profiles to be determined. Additionally, it is possible that beige adipocyte markers are fat depot-specific—that is, pADR, OME, and epicardial fat may not induce the same subset of genes during browning, leading to distinct molecular signatures (39,40). Regardless of the gene expression markers present, our studies of mitochondrial activity definitively demonstrate that pADR fat from pheo^{Multi} patients exhibits a key functional characteristic of brown and beige adipocytes in having enhanced total and uncoupled respiratory activity and up-regulation of genes directly associated with mitochondrial activity. Future studies may reveal whether these genes are also up-regulated in white adipose tissue in other conditions that promote browning.

In conclusion, the phenotypic browning in pADR fat of pheo patients is accompanied by metabolic alterations in mitochondrial activity and related gene expression changes, which could influence fuel utilization and energy expenditure. The induction of browning in pADR from a subset of pheo patients is positively correlated with plasma catecholamines, but additional factors may also contribute. SC and OME fat may not undergo browning in response to chronic adrenergic stress *per se*. Further analyses of the differential gene expression profile and mitochondrial activity in pADR compared to SC and OME fat may shed light on the regulation of browning in pheo pADR adipose tissue, and potential differences between the capacity of human pADR and SC adipose tissues to undergo browning.

Acknowledgements. The authors thank Jennifer Isorena for technical assistance and all the study participants for their contribution.

References

1. **Nedergaard J, Bengtsson T, Cannon B.** Unexpected evidence for active brown adipose

tissue in adult humans. *Am. J. Physiol. Endocrinol. Metab.* 2007;293(2):E444–52.

2. **Cypess AM, Lehman S, Williams G, Tal I, Rodman D, Goldfine AB, Kuo FC, Palmer EL, Tseng Y-H, Doria A, Kolodny GM, Kahn CR.** Identification and importance of brown adipose tissue in adult humans. *N. Engl. J. Med.* 2009;360(15):1509–17.

3. **Virtanen KA, Lidell ME, Orava J, Heglind M, Westergren R, Niemi T, Taittonen M, Laine J, Savisto N-J, Enerbäck S, Nuutila P.** Functional Brown Adipose Tissue in Healthy Adults. *N. Engl. J. Med.* 2009;360(15):1518–1525.

4. **van Marken Lichtenbelt WD, Vanhommerig JW, Smulders NM, Drossaerts JMAFL, Kemerink GJ, Bouvy ND, Schrauwen P, Teule GJJ.** Cold-activated brown adipose tissue in healthy men. *N. Engl. J. Med.* 2009;360(15):1500–8.

5. **Himms-Hagen J.** Brown adipose tissue thermogenesis and obesity. *Prog. Lipid Res.* 1989;28(2):67–115.

6. **Cannon B, Nedergaard J.** Brown adipose tissue: function and physiological significance. *Physiol. Rev.* 2004;84(1):277–359.

7. **Wu J, Boström P, Sparks LM, Ye L, Choi JH, Giang A-H, Khandekar M, Virtanen KA, Nuutila P, Schaart G, Huang K, Tu H, van Marken Lichtenbelt WD, Hoeks J, Enerbäck S, Schrauwen P, Spiegelman BM.** Beige adipocytes are a distinct type of thermogenic fat cell in mouse and human. *Cell* 2012;150(2):366–76.

8. **Petrovic N, Walden TB, Shabalina IG, Timmons JA, Cannon B, Nedergaard J.** Chronic peroxisome proliferator-activated receptor gamma (PPARgamma) activation of epididymally derived white adipocyte cultures reveals a population of thermogenically competent, UCP1-containing adipocytes molecularly distinct from classic brown adipocyt. *J. Biol. Chem.* 2010;285(10):7153–64.

9. **Giordano A, Frontini A, Cinti S.** Convertible visceral fat as a therapeutic target to curb obesity. *Nat. Rev. Drug Discov.* 2016. doi:10.1038/nrd.2016.31.

10. **Seale P, Bjork B, Yang W, Kajimura S, Chin S, Kuang S, Scimè A, Devarakonda S,**

Conroe HM, Erdjument-Bromage H, Tempst P, Rudnicki MA, Beier DR, Spiegelman BM. PRDM16 controls a brown fat/skeletal muscle switch. *Nature* 2008;454(7207):961–7.

11. **Jespersen NZ, Larsen TJ, Peijs L, Daugaard S, Homøe P, Loft A, de Jong J, Mathur N, Cannon B, Nedergaard J, Pedersen BK, Møller K, Scheele C.** A classical brown adipose tissue mRNA signature partly overlaps with brite in the supraclavicular region of adult humans. *Cell Metab.* 2013;17(5):798–805.

12. **Cypess AM, White AP, Vernochet C, Schulz TJ, Xue R, Sass CA, Huang TL, Roberts-Toler C, Weiner LS, Sze C, Chacko AT, Deschamps LN, Herder LM, Truchan N, Glasgow AL, Holman AR, Gavrila A, Hasselgren P-O, Mori MA, Molla M, Tseng Y-H.** Anatomical localization, gene expression profiling and functional characterization of adult human neck brown fat. *Nat. Med.* 2013;19(5):635–9.

13. **Sharp LZ, Shinoda K, Ohno H, Scheel DW, Tomoda E, Ruiz L, Hu H, Wang L, Pavlova Z, Gilsanz V, Kajimura S.** Human BAT possesses molecular signatures that resemble beige/brite cells. *PLoS One* 2012;7(11):e49452.

14. **Sacks HS, Fain JN, Bahouth SW, Ojha S, Frontini A, Budge H, Cinti S, Symonds ME.** Adult epicardial fat exhibits beige features. *J. Clin. Endocrinol. Metab.* 2013;98(9):E1448–55.

15. **Ussar S, Lee KY, Dankel SN, Boucher J, Haering M-F, Kleinridders A, Thomou T, Xue R, Macotela Y, Cypess AM, Tseng Y-H, Mellgren G, Kahn CR.** ASC-1, PAT2, and P2RX5 are cell surface markers for white, beige, and brown adipocytes. *Sci. Transl. Med.* 2014;6(247):247ra103.

16. **Plouin P-F, Gimenez-Roqueplo A-P.** Pheochromocytomas and secreting paragangliomas. *Orphanet J. Rare Dis.* 2006;1:49.

17. **Hondares E, Gallego-Escuredo JM, Flachs P, Frontini A, Cereijo R, Goday A, Perugini J, Kopecky P, Giralt M, Cinti S, Kopecky J, Villarroya F.** Fibroblast growth

factor-21 is expressed in neonatal and pheochromocytoma-induced adult human brown adipose tissue. *Metabolism.* 2014;63(3):312–7.

18. **Betz MJ, Slawik M, Lidell ME, Osswald A, Heglind M, Nilsson D, Lichtenauer UD, Mauracher B, Mussack T, Beuschlein F, Enerbäck S.** Presence of brown adipocytes in retroperitoneal fat from patients with benign adrenal tumors: relationship with outdoor temperature. *J. Clin. Endocrinol. Metab.* 2013;98(10):4097–104.

19. **Di Franco A, Guasti D, Mazzanti B, Ercolino T, Francalanci M, Nesi G, Bani D, Forti G, Mannelli M, Valeri A, Luconi M.** Dissecting the origin of inducible brown fat in adult humans through a novel adipose stem cell model from adipose tissue surrounding pheochromocytoma. *J. Clin. Endocrinol. Metab.* 2014;99(10):E1903–12.

20. **Nagano G, Ohno H, Oki K, Kobuke K, Shiwa T, Yoneda M, Kohno N.** Activation of classical brown adipocytes in the adult human perirenal depot is highly correlated with PRDM16-EHMT1 complex expression. *PLoS One* 2015;10(3):e0122584.

21. **Frontini A, Vitali A, Perugini J, Murano I, Romiti C, Ricquier D, Guerrieri M, Cinti S.** White-to-brown transdifferentiation of omental adipocytes in patients affected by pheochromocytoma. *Biochim. Biophys. Acta* 2013;1831(5):950–9.

22. **Søndergaard E, Gormsen LC, Christensen MH, Pedersen SB, Christiansen P, Nielsen S, Poulsen PL, Jessen N.** Chronic adrenergic stimulation induces brown adipose tissue differentiation in visceral adipose tissue. *Diabet. Med.* 2015;32(2):e4–8.

23. **Huang DW, Sherman BT, Lempicki RA.** Systematic and integrative analysis of large gene lists using DAVID bioinformatics resources. *Nat. Protoc.* 2009;4(1):44–57.

24. **Rogers GW, Brand MD, Petrosyan S, Ashok D, Elorza AA, Ferrick DA, Murphy AN.** High throughput microplate respiratory measurements using minimal quantities of isolated mitochondria. *PLoS One* 2011;6(7):e21746.

25. **Bordicchia M, Liu D, Amri E-Z, Ailhaud G, Dessì-Fulgheri P, Zhang C, Takahashi N, Sarzani R, Collins S.** Cardiac natriuretic peptides act via p38 MAPK to induce the

brown fat thermogenic program in mouse and human adipocytes. *J. Clin. Invest.* 2012;122(3):1022–36.

26. **Strack AM, Bradbury MJ, Dallman MF.** Corticosterone decreases nonshivering thermogenesis and increases lipid storage in brown adipose tissue. *Am. J. Physiol.* 1995;268(1 Pt 2):R183–91.

27. **Stepniakowski K, Januszewicz A, Lapiński M, Feltynowski T, Chodakowska J, Ignatowska-Switalska H, Wocial B, Januszewicz W.** Plasma atrial natriuretic peptide (ANP) concentration in patients with pheochromocytoma. *Blood Press.* 1992;1(3):157–61.

28. **Waldén TB, Hansen IR, Timmons JA, Cannon B, Nedergaard J.** Recruited vs. nonrecruited molecular signatures of brown, "brite," and white adipose tissues. *Am. J. Physiol. Endocrinol. Metab.* 2012;302(1):E19–31.

29. **Svensson P-A, Jernås M, Sjöholm K, Hoffmann JM, Nilsson BE, Hansson M, Carlsson LMS.** Gene expression in human brown adipose tissue. *Int. J. Mol. Med.* 2011;27(2):227–32.

30. **Shinoda K, Luijten IHN, Hasegawa Y, Hong H, Sonne SB, Kim M, Xue R, Chondronikola M, Cypess AM, Tseng Y-H, Nedergaard J, Sidossis LS, Kajimura S.** Genetic and functional characterization of clonally derived adult human brown adipocytes. *Nat. Med.* 2015;21(4):389–94.

31. **de Jong JMA, Larsson O, Cannon B, Nedergaard J.** A stringent validation of mouse adipose tissue identity markers. *Am. J. Physiol. Endocrinol. Metab.* 2015;308(12):E1085–105.

32. **Chondronikola M, Volpi E, Børsheim E, Porter C, Annamalai P, Enerbäck S, Lidell ME, Saraf MK, Labbe SM, Hurren NM, Yfanti C, Chao T, Andersen CR, Cesani F, Hawkins H, Sidossis LS.** Brown adipose tissue improves whole-body glucose homeostasis and insulin sensitivity in humans. *Diabetes* 2014;63(12):4089–99.

33. **van der Lans AAJJ, Hoeks J, Brans B, Vijgen GHEJ, Visser MGW, Vosselman MJ,**

Hansen J, Jörgensen JA, Wu J, Mottaghy FM, Schrauwen P, van Marken Lichtenbelt WD. Cold acclimation recruits human brown fat and increases nonshivering thermogenesis. *J. Clin. Invest.* 2013;123(8):3395–403.

34. **Sidossis LS, Porter C, Saraf MK, Børsheim E, Radhakrishnan RS, Chao T, Ali A, Chondronikola M, Mlcak R, Finnerty CC, Hawkins HK, Toliver-Kinsky T, Herndon DN.** Browning of Subcutaneous White Adipose Tissue in Humans after Severe Adrenergic Stress. *Cell Metab.* 2015;22(2):219–27.

35. **Patsouris D, Qi P, Abdullahi A, Stanojcic M, Chen P, Parousis A, Amini-Nik S, Jeschke MG.** Burn Induces Browning of the Subcutaneous White Adipose Tissue in Mice and Humans. *Cell Rep.* 2015;13(8):1538–44.

36. **Kern PA, Finlin BS, Zhu B, Rasouli N, McGehee RE, Westgate PM, Dupont-Versteegden EE.** The effects of temperature and seasons on subcutaneous white adipose tissue in humans: evidence for thermogenic gene induction. *J. Clin. Endocrinol. Metab.* 2014;99(12):E2772–9.

37. **Leibel RL, Edens NK, Fried SK.** Physiologic basis for the control of body fat distribution in humans. *Annu. Rev. Nutr.* 1989;9:417–43.

38. **Lidell ME, Betz MJ, Dahlqvist Leinhard O, Heglind M, Elander L, Slawik M, Mussack T, Nilsson D, Romu T, Nuutila P, Virtanen KA, Beuschlein F, Persson A, Borga M, Enerbäck S.** Evidence for two types of brown adipose tissue in humans. *Nat. Med.* 2013;19(5):631–4.

39. **Kajimura S, Spiegelman BM, Seale P.** Brown and Beige Fat: Physiological Roles beyond Heat Generation. *Cell Metab.* 2015;22(4):546–559.

40. **Cypess AM, Haft CR, Laughlin MR, Hu HH.** Brown fat in humans: consensus points and experimental guidelines. *Cell Metab.* 2014;20(3):408–15.

Figure Legends

Figure 1. Histomorphology of white adipose tissue depots. Representative images of H&E stained sections from pADR, SC, and OME fat of control and pheo patients. Multilocular adipocytes were present exclusively in pADR fat, and observed in 4% and 52.4% of control and pheo patients, respectively (10x magnification. Black bar represents 100 μm).

Figure 2. Plasma catecholamine levels in control and pheo patients. Pheo^{Multi} patients show the highest catecholamine levels. * $P < 0.05$, ** $P < 0.01$, *** $P < 0.001$. Data analyzed by Kruskal-Wallis multiple comparison test, except for total catecholamine levels where a one-way ANOVA multiple comparison test was used (n = 10-25).

Figure 3. Detection of UCP1 in pADR fat. A: UCP1 mRNA levels in pADR (n = 8-20), SC (n = 6-20) and OME (n = 2-5) fat. ** $P < 0.01$, *** $P < 0.001$ using a one-way ANOVA multiple comparison test. B: Immunohistochemistry using an antibody against UCP1. Positive staining was present only in the multilocular adipocytes from pADR fat (10x magnification. Black bar represents 100 μm). C: UCP1 protein in pADR fat detected by Western blot. Ponceau red stain of total protein is shown for normalization.

Figure 4. Mitochondrial respiration is increased in pheo^{Multi} pADR fat. A: Complex II-driven oxygen consumption rate (OCR) in isolated mitochondria from pADR (n = 8-12), SC (n = 5-10), and OME (n = 2-3) fat depots. B: mitochondrial respiration parameters from a coupling assay. Complex V and maximal respiration were obtained after sequentially injections of ADP and FCCP, respectively. Coupled respiration was the oligomycin-sensitive OCR while uncoupled was the OCR difference between oligomycin and antimycin A injections (n = 8-12). C: different electron transport chain complexes respiration. Complex I, II, and IV respiration were measured

after the sequential injection of pyruvate, succinate and ascorbate/TMPD, respectively. Complex III respiration corresponded to the antimycin A-sensitive respiration (n = 5-12). * $P < 0.05$, ** $P < 0.01$, *** $P < 0.001$. Data analyzed by Kruskal-Wallis multiple comparison test.

Figure 5. Gene expression profiling of pADR fat from control, pheo^{Uni} and pheo^{Multi} subjects by microarray analysis.. A: Left, Venn diagrams illustrating the genes up- and down-regulated in pADR fat from pheo^{Uni} and pheo^{Multi} compared to control subjects. Right, functional enrichment analysis of genes that are uniquely up- or down-regulated in the pheo^{Multi} group, using DAVID analysis with SP_PIR categories. The number of genes for each functional category (Count), enrichment *P* values, and multiple testing correction (Benjamini < 0.0001 and <0.05 for up- and down-regulated genes, respectively) are presented. B: Heat map representation of gene expression levels for genes in the top SP_PIR category ("mitochondrion") genes that are up-regulated in the pheo^{Multi} group. Genes are presented in alphabetical order. C: Validation of 5 electron transport genes up-regulated in pADR pheo^{Multi} by RT-qPCR or Western blot. * $P < 0.05$, ** $P < 0.01$ using a one-way ANOVA multiple comparison test (n = 7-20).

Table 1. Characteristics of subjects used in the study.

	Control subjects	All pheo	$Pheo^{Uni}$	$Pheo^{Multi}$
Age (years)	53.4 ± 8.2	51.2 ± 13.4	47.1 ± 13.6	54.9 ± 12.7
Male/Female (n)	15/10	9/12	4/6	5/6
BMI (kg/m^2)	30.3 ± 7.1	26.6 ± 4.5*	27.7 ± 5.6	25.7 ± 3.4
Glucose (mg/dl)	88.9 ± 35.5	78.6 ± 12.8	84.1 ± 15.7	74.1 ± 7.9
FFA (mmol/l)	0.73 ± 0.40	0.54 ± 0.30	0.47 ± 0.15	0.58 ± 0.34
ANP (pg/ml)	33.0 ± 10.2	32.2 ± 4.2	31.9 + 8.3	32.4 ± 1.1
BNP (pg/ml)	116 ± 81	134 ± 88	177 ± 91	102.3 ± 77
Cortisol (µg/dl)	11.5 ± 3.1	9.2 ± 3.5	9.3 ± 4.9	9.0 ± 2.0

Data are expressed as mean ± SD. FFA, free fatty acid, ANP, atrial natriuretic peptide; BNP, B-type natriuretic peptide. ***** $P < 0.05$ vs control.

Figure 1

Click here to download Figure Fig1

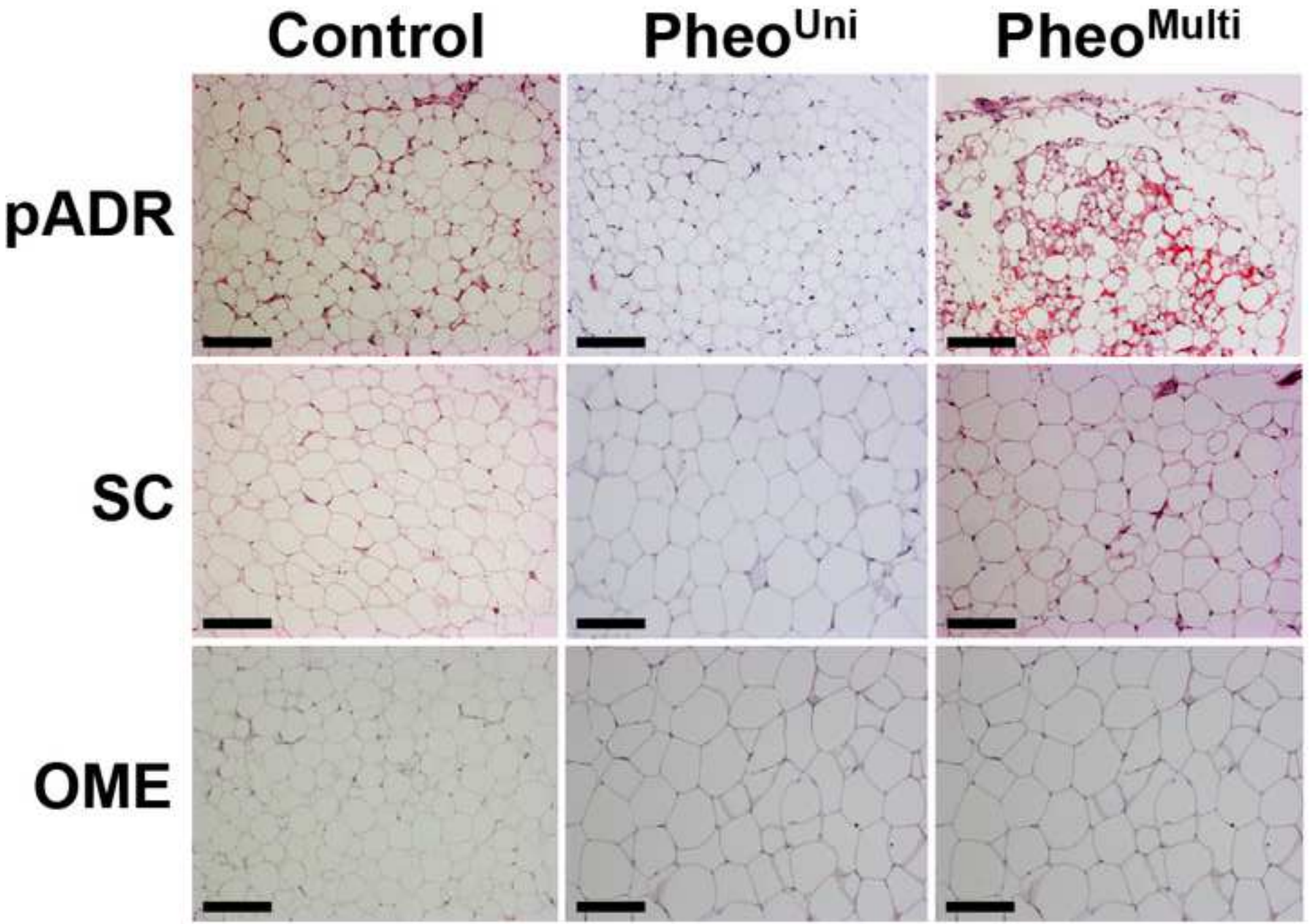

Figure 2

Click here to download Figure Fig2

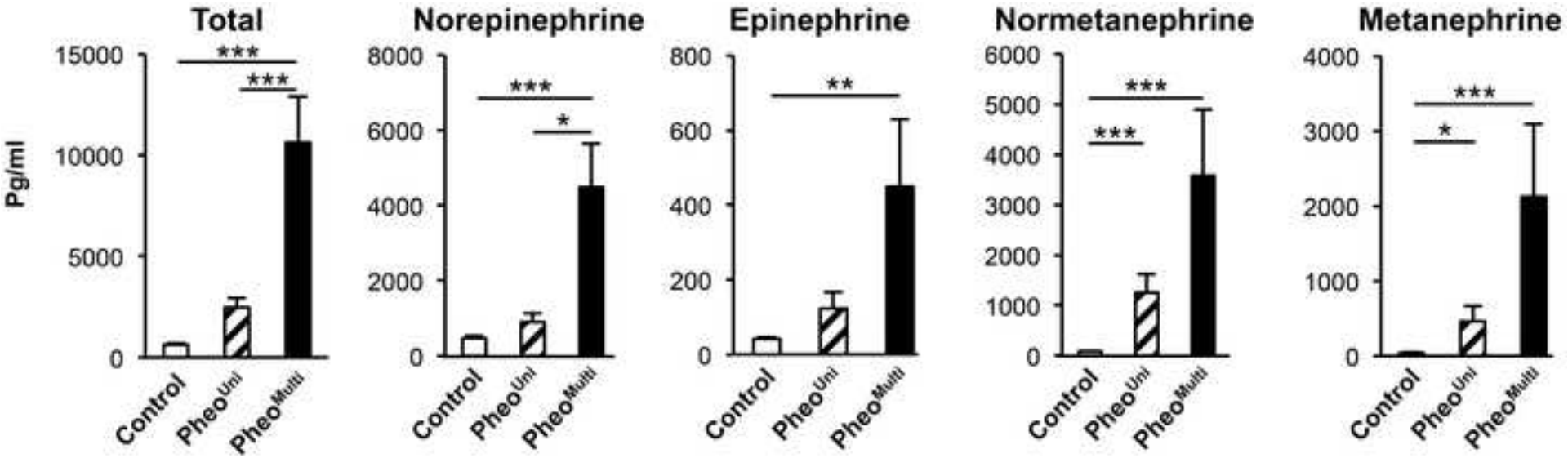

Figure 3

Click here to download Figure Fig3

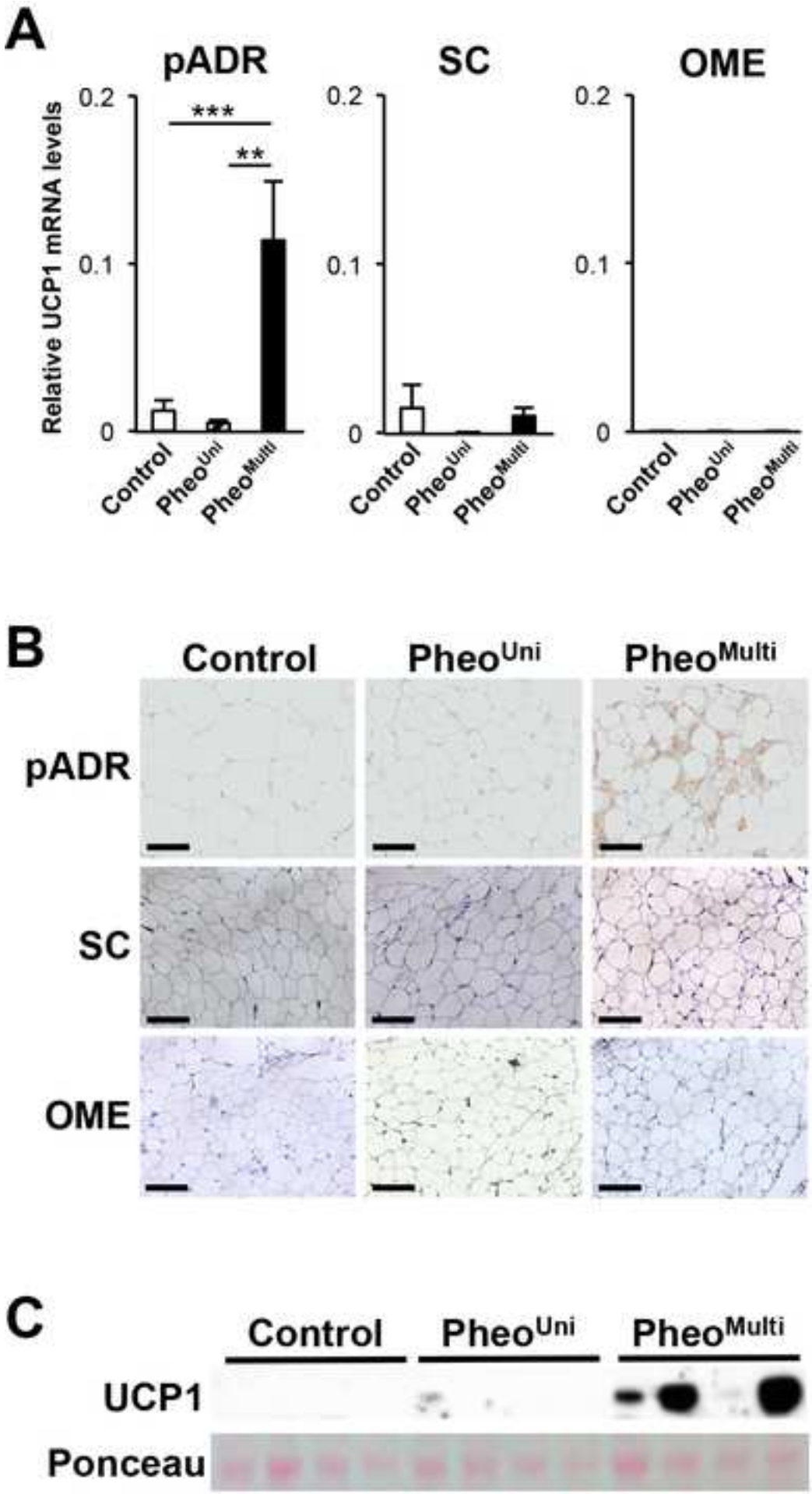

Figure 4

Click here to download Figure Fig4

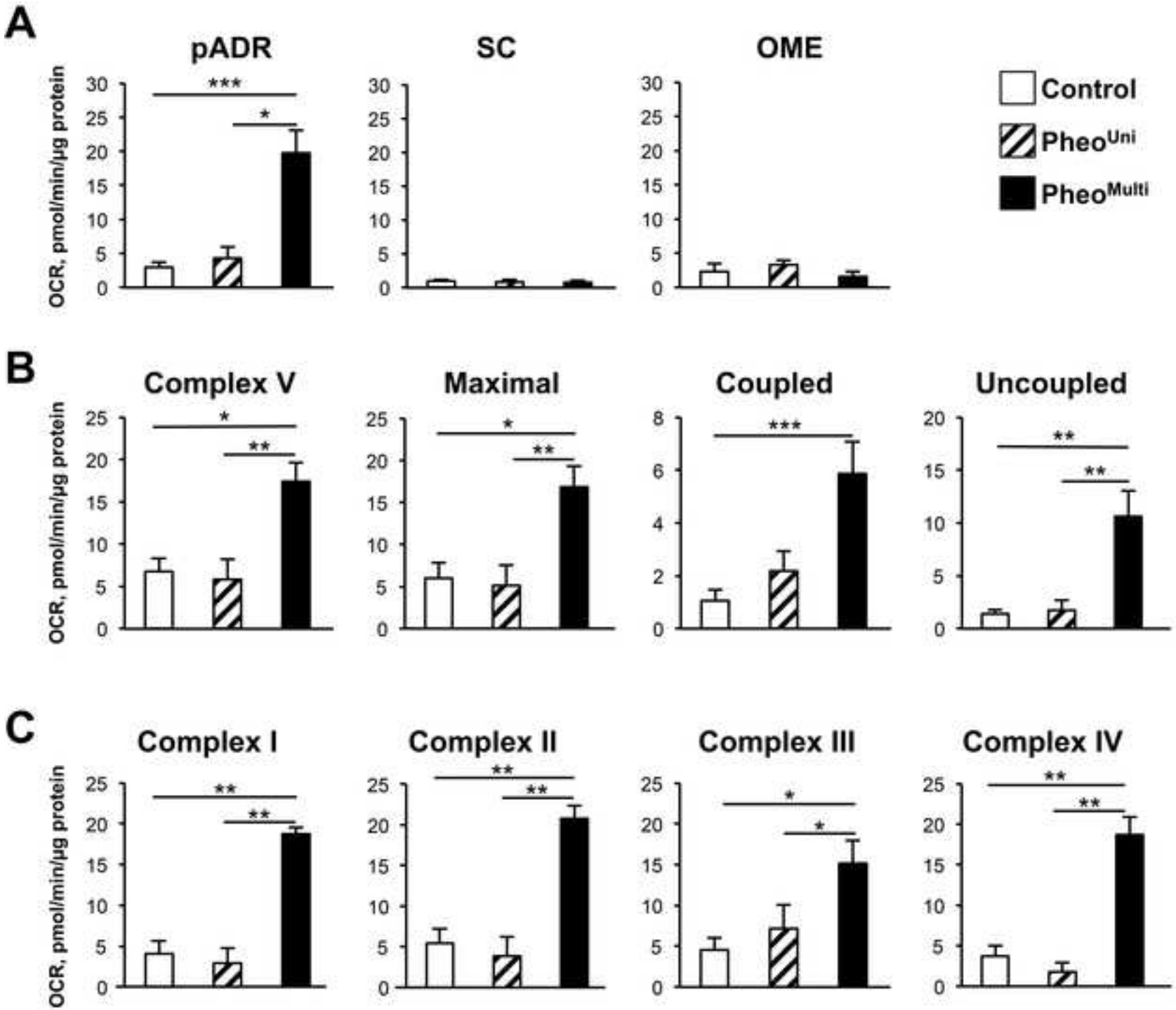

Figure 5

Click here to download Figure Fig5

A

Up-regulated

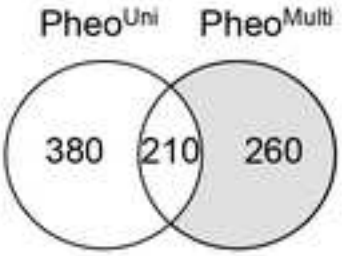

Category	Term	Count	*P* value	Benjamini
SP_PIR_KEYWORDS	Mitochondrion	82	1.82E-48	1.82E-48
SP_PIR_KEYWORDS	Transit peptide	54	1.39E-35	6.95E-36
SP_PIR_KEYWORDS	Mitochondrion inner membrane	28	1.43E-20	4.78E-21
SP_PIR_KEYWORDS	Oxidoreductase	30	1.27E-09	3.17E-10
SP_PIR_KEYWORDS	Respiratory chain	12	1.27E-08	2.53E-09
SP_PIR_KEYWORDS	Electron transport	12	1.03E-06	1.72E-07
SP_PIR_KEYWORDS	Lipid metabolism	14	4.42E-06	6.31E-07
SP_PIR_KEYWORDS	Fatty acid metabolism	10	9.09E-06	1.14E-06
SP_PIR_KEYWORDS	Flavoprotein	11	1.01E-04	1.12E-05
SP_PIR_KEYWORDS	FAD	11	1.84E-04	1.84E-05

Down-regulated

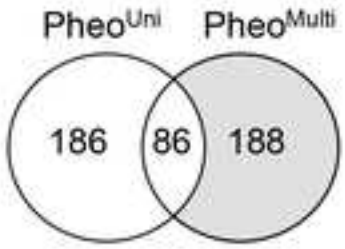

Category	Term	Count	*P* value	Benjamini
SP_PIR_KEYWORDS	Signal	47	0.003	0.003
SP_PIR_KEYWORDS	Secreted	29	0.019	0.009
SP_PIR_KEYWORDS	Disulfide bond	41	0.023	0.008
SP_PIR_KEYWORDS	Cytokine	9	0.023	0.006
SP_PIR_KEYWORDS	Heparin-binding	6	0.041	0.008

B

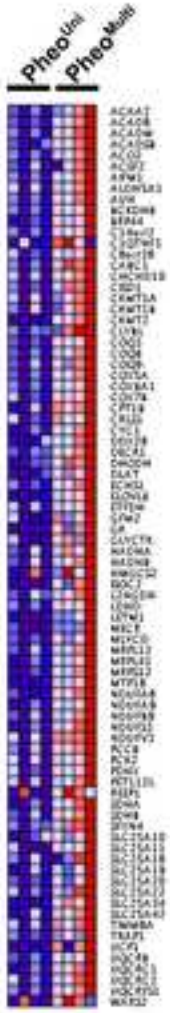

C

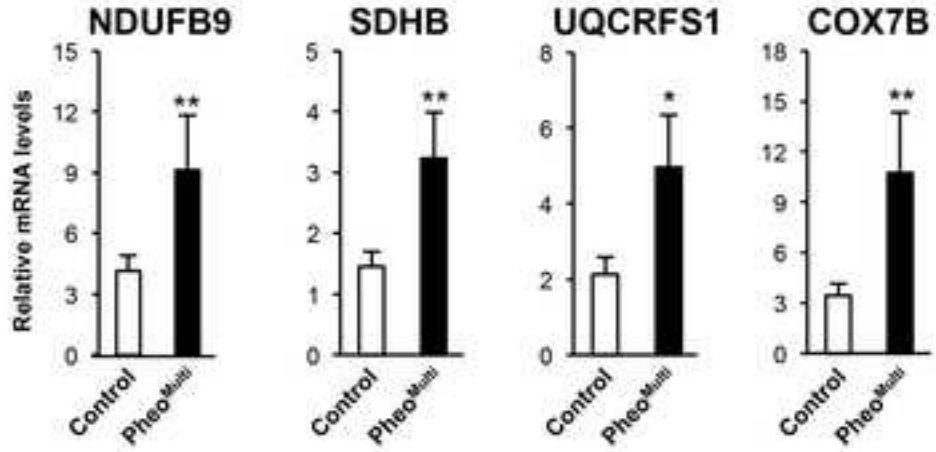

Supplemental Table 2

Supplemental Fig. 1